# Electronic Supplementary Information

## Theoretical Investigations on the Charge Transport Properties of the Anthracene Derivatives with Aryl Substituents at the 2,6-Position—Thermal Stable "herringbone" Stacking Motif

Xiao-Qi Sun [a], Gui-Ya Qin [b], Pan-Pan Lin [b], Jin Wang [a], Jian-Xun Fan [c], Hui-Yuan Li [b], Ai-Min REN* [b], Jing-Fu Guo* [a]

Correspondence to: Jing-Fu Guo (E-mail: guojf217@nenu.edu.cn)
Ai-Min Ren (E-mail: aimin_ren@yahoo.com)

[a] *School of Physics, Northeast Normal University, Changchun, 130024, China*

[b] *Laboratory of Theoretical and Computational Chemistry, Institute of Theoretical Chemistry, Jilin University, Changchun, 130023, PR China*

[c] *College of Chemistry and Life Science, Weinan Normal University, Weinan 714000, China*

## Contents

**Fig S9.** $E_{SCS\text{-}SAPT0}$ and $E_{elec}$, $E_{ind}$, $E_{disp}$, and $E_{exch}$ of the b-b and s-s.

**Section1.**

Considering the influence of oxygen atoms in the BDBFAnt, we calculated the λs of several anthracene derivatives without heteroatoms (2,6-trianthrylene and 2,6-ditetraceneanthracene), which are shown in **Fig S1**. The calculation is based on results in the gas phase due to the absence of crystal structures, with the substituent growing, both the HF and the LF areas vibration contribution to the $\lambda_h$s decreases. Meanwhile, doping of oxygen atoms increases the contribution to the λ in the HF area slightly, mainly around at the frequency of 1577.59$cm^{-1}$ and arises from carbon atoms stretching motion and hydrogen atom scissoring motion in-plane. Hence, the oxygen atom in the substituent increases the hole reorganization energy, and it can be excluded that the heteroatom doping causes the decrease of reorganization energy, so we conclude that the vibrational contribution to the reorganization energy gradually decreases as the 2,6-site aryl substituents chain length increasing.

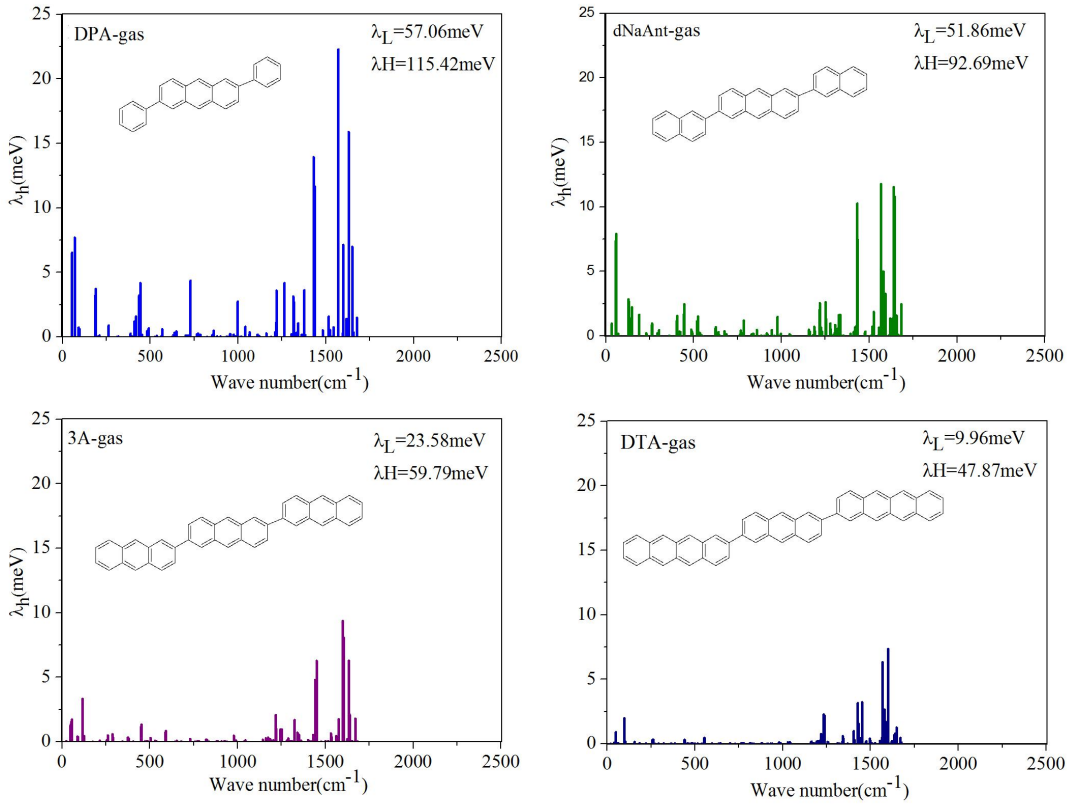


**Fig S1.** Contributions of each vibrational mode to hole reorganization energies in gas phase for

DPA, dNaAnt, 3A, DTA.

From **Fig S2**, it can be seen that the $\lambda_e$s in the solid phase gradually decrease with the extension of 2,6-aryl substituents. The magnitude of the $\lambda_e$s in the LF region is summed as: $\lambda_{Anthracene}$=60.91meV, $\lambda_{DPA}$=41.64meV, $\lambda_{dNaAnt}$=38.29meV, $\lambda_{BDBFAnt}$=27.95meV, and the magnitude of the $\lambda e$ in the HF range is summed as: $\lambda_{Anthracene}$=137.72meV, $\lambda_{DPA}$=136.9meV, $\lambda_{dNaAnt}$=138.66meV, $\lambda_{BDBFAnt}$=142.8meV. It can be found that the $\lambda_e$s decrease more drastically in the LF region with the extension of the 2,6-aryl substituent, while there is little difference in the contribution to the $\lambda_e$s in the HF range, so the vibrational contribution in the LF areas to the $\lambda_e$ is more distinctive, dominating the order of the $\lambda_e$ values for the studied compounds.

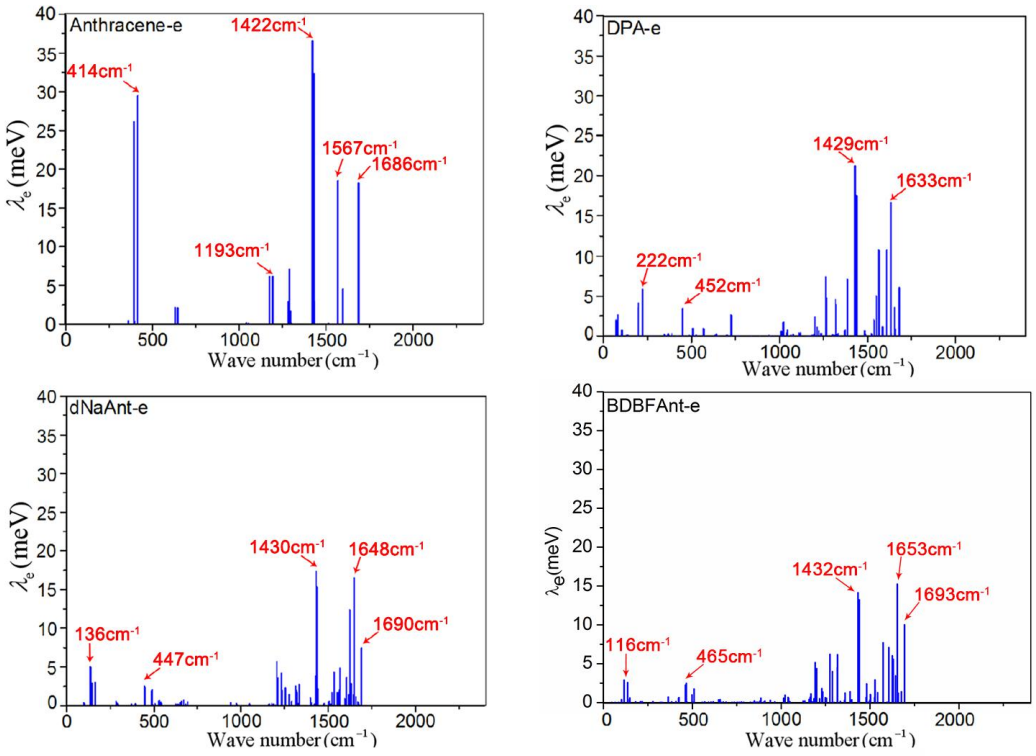


**Fig S2.** Contributions of each vibrational mode to electron reorganization energies under QM/MM geometries for all the molecules studied.

**Section2.**

After substituting, the intermolecular vertical distance decrease, and the horizontal slipped distance increase ($s_{Anthrancene}$=2.680Å, $s_{DPA}$=3.086Å, $s_{dNaAnt}$=2.763Å, $s_{BDBFAnt}$=2.805Å) as shown in **Fig S3** due to intermolecular non-covalent interactions. So the substitution at 2,6-site of anthracene causes a reduction in both the $V_h$ and $V_e$ values for face-to-face stacking dimers (DPA<BDBFAnt<dNaAnt<Anthracene). Obviously, the face-to-face transport path in DPA has a significant small $V_h$ value due to huge horizontal slipped distance.

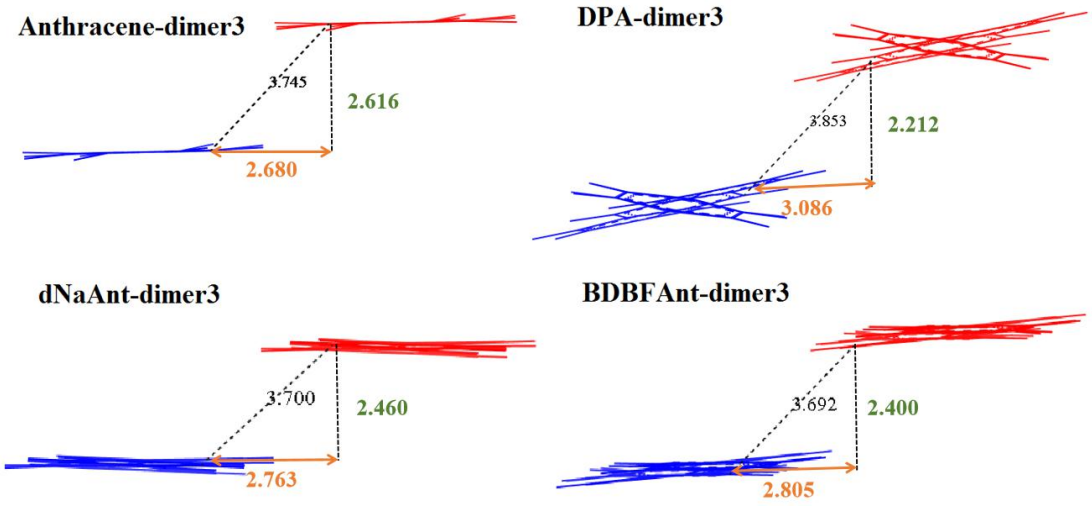


**Fig S3.** Stacking and spatial position of face-to-face molecular dimers in anthracene and anthracene derivatives, with vertical distances in green and horizontal sliding distances in yellow, and the unit of the distance is Å.

**Section3.**

We calculated the interaction energies and corresponding energy decomposition of the next closest dimers (path**3**, path**2**, **3** of the dNaAnt) to make our conclusion more comprehensive and credible. From **Table S1**, it can be found that the electrostatic term is dominant and the induction term is smaller, which is similar to the edge-to-face dimers. Simultaneously, the total interaction energy $E_{SCS\text{-}SAPT0}$ is less than that of the edge-to-face dimers, indicating that the edge-to-face dimers of the herringbone is more stable. Therefore, we focus on careful analysis and discussion of this pair of dimers in the main text.

**Table S1.** Molecular interaction energy and corresponding energy decomposition of the next closest dimers (path**3**, path**2**, **3** of the dNaAnt). $E_{elec}$, $E_{ind}$, $E_{disp}$ and $E_{exch}$ are the electrostatic, induction, dispersion and exchange repulsion energies (in kcal/mol), respectively. The brackets represent the percentage of the total energy.

| | $E_{SCS\text{-}SAPT0}$ | $E_{elec}$ | $E_{ind}$ | $E_{disp}$ | $E_{exch}$ |
|---|---|---|---|---|---|
| Anthracene | -6.27 | -3.61 | -0.77 | -7.26 | 5.37 |
| | | -21.25% | -4.52% | -42.68% | 31.57% |
| DPA | -9.32 | -3.27 | -0.57 | -9.29 | 3.83 |
| | | -19.29% | -3.39% | -54.77% | 22.55% |
| dNaAnt-dimer3 | -15.50 | -7.14 | -1.30 | -17.16 | 10.10 |
| | | -20.00% | -3.65% | -48.06% | 28.29% |
| BDBFAnt | -16.45 | -6.48 | -1.37 | -18.12 | 9.53 |
| | | -18.27% | -3.85% | -51.04% | 26.84% |
| dNaAnt-dimer2 | -23.07 | -8.67 | -2.17 | -29.63 | 17.39 |
| | | -14.98% | -3.74% | -51.21% | 30.07% |

**Section4.**

To better illustrate the influence of oxygen atoms in BDBFAnt, we replaced the oxygen atoms with $CH_2$ (2, 6-difluorenylanthrancene DFA) and optimized the newly added carbon and hydrogen atoms based on the BDBFAnt lattice and the arrangement of the molecules. The molecular structure or crystal structure is shown in **Fig S4**. The total interaction energy ($E_{SCS\text{-}SAPT0}$) of DFA was obtained, and almost unchanged compared to BDBFAnt (25.93-25.90 kcal/mol), whereas the sub-energies all increased. The above conjecture is also verified that the oxygen atoms decrease the sub-energies ($E_{elec}$, $E_{ind}$, and $E_{exch}$) , so that the $E_{SCS\text{-}SAPT0}$s as well as the sub-energies of the anthracene derivatives without heteroatoms will grow with the increase of substituents.

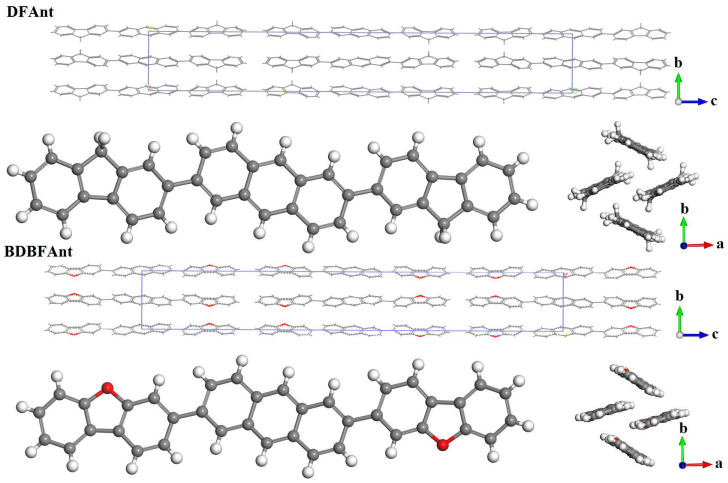


**Fig S4.** The single molecule molecular structure and crystal stacking of DFAnt and BDBFAnt.

**Table S2.** Molecular interaction energy and corresponding energy decomposition of the closest dimers of BDBFAnt and DFAnt. Eelec, Eind, Edisp, and Eexch are the electrostatic, induction, dispersion and exchange repulsion energies (in kcal/mol), respectively. The brackets represent the percentage of the total energy.

| | $E_{elec}$ | $E_{ind}$ | $E_{disp}$ | $E_{exch}$ | $E_{SCS\text{-}SAPT0}$ |
|---|---|---|---|---|---|
| BDBFAnt | -8.46 (13.79%) | -2.30 (3.75%) | -32.89 (53.59%) | 17.72 (28.87%) | -25.93 |
| DFAnt | -13.65 (15.65%) | -3.98 (4.56%) | -38.92 (44.64%) | 30.64 (35.15%) | -25.90 |

**Section5.**

Based on the edge-to-face dimer models of DPA at different angles, the intermolecular interactions of the dimer models are calculated to obtain the idealized stable dimers. The results are shown in **Fig S5**, where the most stable stacking of dimers can be found at 39.5°, which is very close to the actual stacking of crystals. When it is less than 39.5°, the π-π interaction in the backbone will increase, resulting in the repulsive term being greater than the electrostatic term, while when the dihedral angle is larger than 39.5°, the increase in C-H-π interaction makes the proportion of electrostatic attraction larger than the exchange repulsion term. From **Fig S5(b)**, the changes in the proportions of the electrostatic term will decrease as the dihedral angle increases.

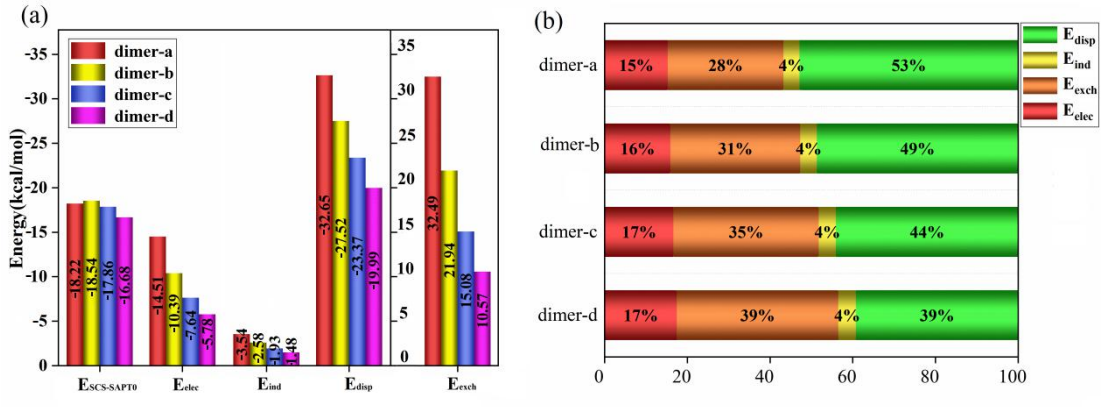


**Fig S5. (a)** Molecular interaction energy and corresponding energy decomposition of the nearest neighboring molecule of edge-to-face dimers of DPA after changing the dihedral angle between anthracene-cores in the dimer (The included angles of a, b, c, d are 37.5°, 39.5°, 41.5°, 43.5°, respectively). **(b)** The percentage of the sub-energies in the total energy. $E_{exch}$, $E_{ind}$, $E_{disp}$, and $E_{exch}$ are the electrostatic, induction, dispersion and exchange repulsion energies (in kcal/mol), respectively.

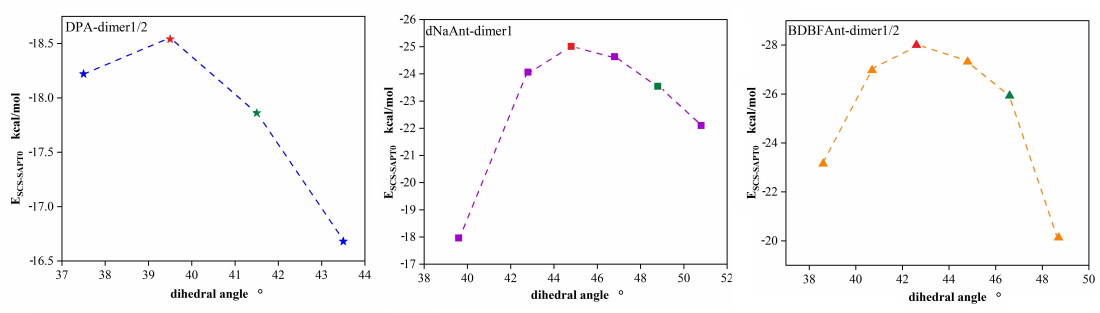


**Fig S6.** The relationship between the total intermolecular interaction energy $E_{SCS\text{-}SAPT0}$ (in kcal/mol) and the dihedral angle of edge-to-face dimers of DPA, dNaAnt, BDBFAnt, and the red is the most stable dihedral angle of the dimer, and the green is the dihedral angle in the actual crystal.

**Section6.**

For the purpose of describing the intermolecular interaction more intuitively, Hirshfeld surface and 2D Fingerprint Plots analysis is performed on the molecular crystal structure (**Table 5** and **Fig S7**). For BDBFAnt, the incorporation of the oxygen atoms in the aromatic ring substituents reduces the contacts between H···H and C···H, and the contact of O···C/H/O increases, accordingly. Besides, we can see that the percentage of C···C contact is rarely 1.7%, 1.3%, 0.7%, and 1.1% for anthracene derivatives. Combining with the shape index in **Fig S8**, it can be found that there are little π···π contacts between $sp^2$ C of two molecules in this series of molecules. Furthermore, the intermolecular interaction force at the bond linkage between the anthracene-core and the substituents in the DPA is powerful. Therefore, a certain dihedral angle is formed between the anthracene core and the aryl substituent in DPA. It can also be seen from **Table 5** and **Fig S7** that the intermolecular interactions are mainly dominated by the CH···π interactions, as shown the intermolecular contact types are mainly divided as C···H contact (around 50% to 60%), H···H contact (around 30% to 50%) and O···C/H/O contact (around 10%, only for BDBFAnt).

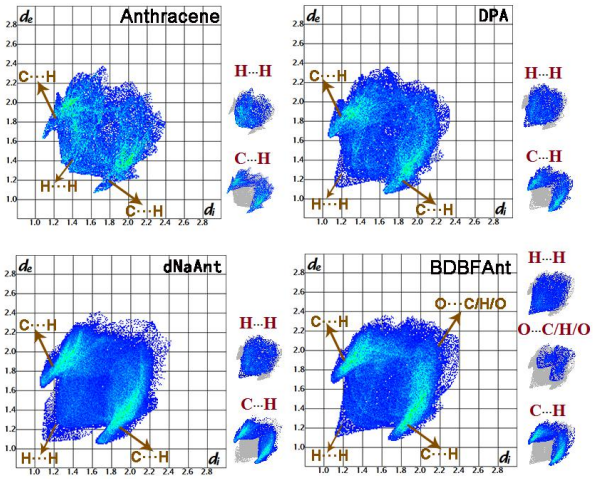


**Fig S7.** The 2D Fingerprint Plots for several crystal structures. (di/de represents the distances from the Hirshfeld surface to the nearest atoms inside/outside the surface).

**Section7**.

Combining with the shape index in **Fig S8**, it can be found that there is almost no π···π interaction between $sp^2$ C of two molecules. **Fig S7** can be utilized for visualization and analysis of non-covalent interactions in molecular crystals, where the normalized contact distance defined as $d_{norm} = \frac{d_i - r_i^{vdW}}{r_i^{vdW}} + \frac{d_e - r_{ei}^{vdW}}{r_e^{vdW}}$, can identify unique and significant intermolecular contact distances, the $r_{i/e}^{vdW}$ represents van der Waals radius, $d_{i/e}$ is the distance from the Hirshfeld surface to the nearest atoms inside/outside surface. The red zone indicates important intermolecular contacts where the distance between the inner and outer nearest atoms is less than the sum of the Van-der-Waals-Radius. It can be found that the intermolecular interaction force at the bond linkage between the anthracene-core and the substituents in the DPA is powerful. Therefore, a certain dihedral angle is formed between the anthracene nucleus and the aryl substituent in DPA.

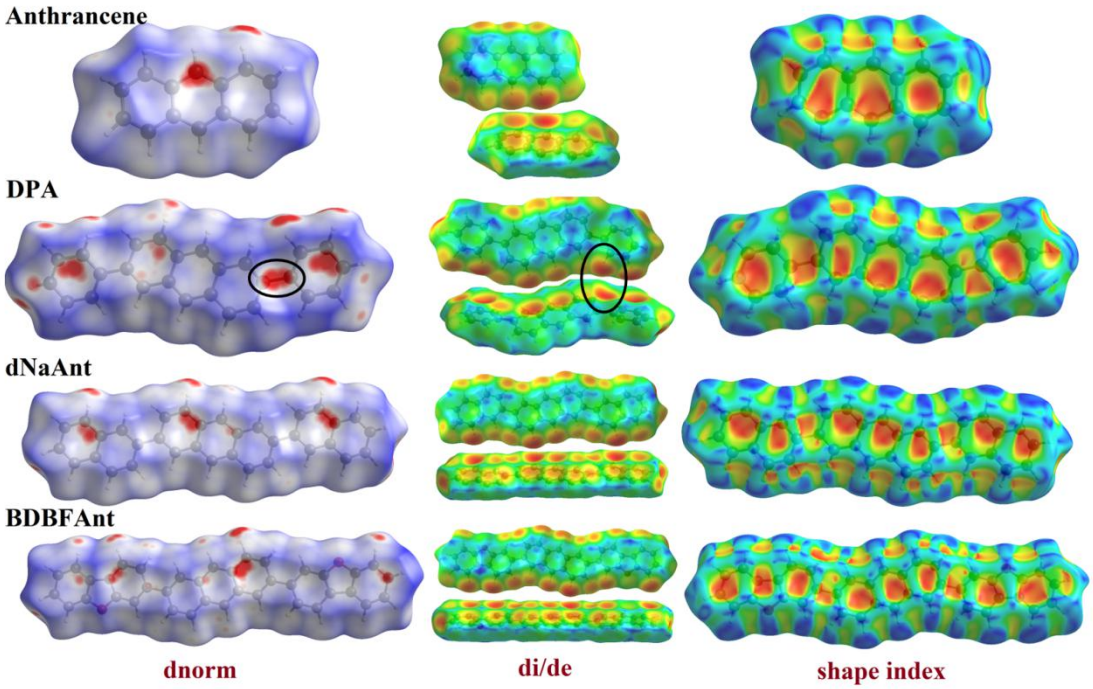


**Fig S8**. The Hirshfeld surface of molecules in single crystals mapped with dnorm surface, di / de surface and shape index (SI).

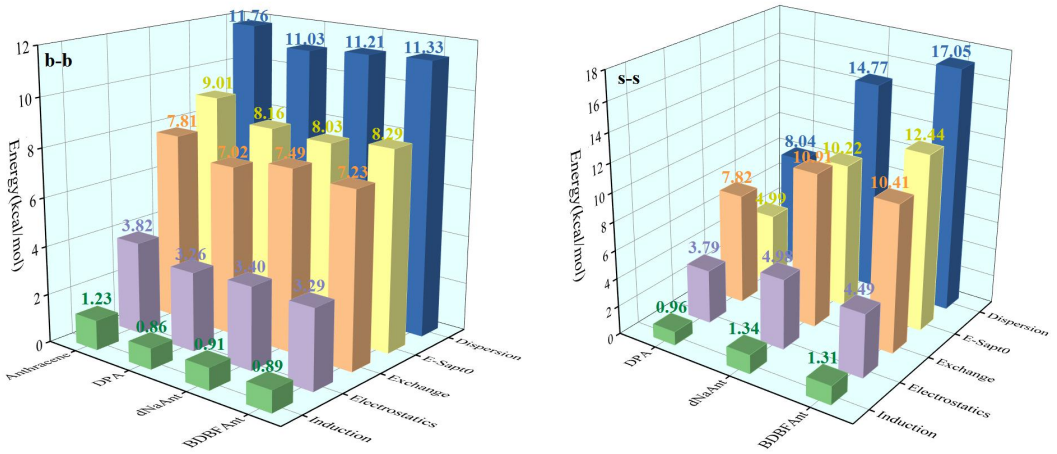


**Fig S9.** Intermolecular interaction energy ($E_{SCS\text{-}SAPT0}$) for the edge-to-face dimers and the energy decomposition ($E_{elec}$, $E_{ind}$, $E_{disp}$, and $E_{exch}$) corresponding interaction energy between the backbone and the backbone (b-b) as well as between substituent and substituent (s-s). All calculations were performed at the SCS-SAPT0/jun-cc-pvdz level.